



Evidence for deep gas loss in open volcanic systems

Marielle Collombet¹ · Alain Burgisser¹ · Mathieu Colombier² · Elizabeth Gaunt³

Received: 18 August 2020 / Accepted: 31 December 2020 / Published online: 16 January 2021
© International Association of Volcanology & Chemistry of the Earth's Interior 2021

Abstract

Previous studies of Vulcanian eruptive products have shown that the respective volcanic conduits were filled for the most part with low-porosity magma (i.e., < 10 vol%) prior to eruption. Comparison with the theoretical porosity distribution expected from closed-system degassing suggests that gas loss must have taken place at depth within the magmatic column (between 3 and 5 km). At such high pressures (between 70 and 110 MPa), however, porosities are low enough (< 20 vol%) to rule out traditional gas loss mechanisms. We tested if channelling, an outgassing mechanism based on bubble connection due to high crystal content (>40 vol%) proposed to occur in mushy magma reservoirs, could also happen in volcanic conduits. We reanalyzed phenocryst, microlite, and porosity data from recent eruptions of Merapi volcano, Indonesia, Soufrière Hills volcano, Montserrat, and Tungurahua volcano, Ecuador. Overall, these magmas had crystal contents high enough for outgassing to occur by channelling. Gases could be channelled out of the magma columns at various levels during ascent to yield mostly gas-depleted magma columns prior to explosive behavior. Such outgassing by channelling thus has the capacity to influence eruptive style. Depending on the phenocryst content, microlite growth during ascent can either foster or impede gas escape by channelling. Considering the pervasive occurrence of microlites and ensuing high crystal contents in volcanic conduits (between 40 and 70 vol%), the high likelihood of channelling implies that other outgassing mechanisms might not be as dominant as previously envisioned.

Keywords Silicic volcanoes, · Outgassing, · Crystal content, · Channelling, · Porosity

Introduction

The eruption of viscous magma at the Earth's surface often gives rise to abrupt regime changes, such as the transition from the gentle effusion of a lava dome to brief but powerful Vulcanian explosions. These eruptive regimes are controlled by outgassing, a process by which the gas contained in bubbles formed during ascent can escape from the magma. In the case of highly viscous magmas (viscosity $>10^6$ Pa.s), individual bubbles are trapped within the melt and cannot migrate individually through the magmatic column, hindering the bubbly flow outgassing mechanism

that is generally at play for low viscosity magmas (Parmigiani et al. 2016; Cardoso and Woods, 1999). Gas loss within highly viscous magmas is mainly related to bubble connectivity and to percolation, which controls the ability for the gas to travel through these bubble connections, making the magma permeable under specific physical conditions. Favorable physical conditions for percolation to occur depend on the amount, size, and shape of the bubbles, deformation, which promotes bubble connectivity (e.g., Blower 2001; Rust and Cashman 2004; Burgisser et al. 2017; Kushnir et al. 2017), and the presence of crystals (Lindoo et al. 2017; deGraffenried et al. 2019; Degruyter et al. 2019; Colombier et al. 2020). In some cases, brittle failure and cracks can also appear (Shields et al. 2014). When quantified, permeabilities deduced from the combination of these parameters range between 10^{-15} and 10^{-12} m² (e.g., Klug and Cashman, 1996; Farquharson et al. 2015; Kushnir et al. 2016; Burgisser et al. 2017). When integrated into numerical models, they contribute to reproduce effusive regimes that are compatible with field observations like preserved vesicularity population described on an eroded conduit, or extrusion rate during dome-forming activity (e.g., Melnik and Sparks, 2002; Collombet, 2009; Degruyter et al. 2012; Cassidy et al. 2018).

Editorial responsibility: K.V. Cashman

✉ Marielle Collombet
marielle.collombet@univ-smb.fr

¹ Univ. Grenoble Alpes, Univ. Savoie Mont Blanc, CNRS, IRD, UGE, ISTerre, 38000 Grenoble, France

² Department of Earth and Environmental Sciences, Ludwig-Maximilians-Universität, München, Germany

³ Instituto Geofísico, Escuela Politécnica Nacional, Quito, Ecuador

However, these numerical models fail to reproduce the very low porosity values inferred to occur in the conduit prior to Vulcanian eruptions. Figure 1 shows the porosity distribution prior to the Vulcanian explosion on February 10, 2010 at Soufrière Hills volcano, Montserrat (Burgisser et al. 2019). Samples collected in the field provide porosity data down to approx. 70 MPa (~3 km depth) that are significantly below the theoretical porosities suggested for a closed system. The outgassing mechanisms, which are based on bubble connection relationships implemented in various numerical models, could explain low porosity values near the surface but fail to reproduce porosity values at depth (beyond a corresponding pressure of 10 MPa). This implies that another outgassing mechanism is at play and/or that a large amount of gas has been evacuated from the deepest parts of the magma column (most likely above 70 MPa) during and/or before the ascent from the reservoir.

We test the hypothesis that this mismatch is due to a missing physical mechanism that greatly enhances outgassing efficiency within the conduit, even at very low porosity values (<10 vol%). This mechanism, channelling, which involves a rigid crystal framework, was first described for the case of magma chambers by Parmigiani et al. (2017) and Degruyter et al. (2019). Channelling relies on the capacity of crystal-rich magmas to build sustainable channels for gas percolation independently from magma movements. For crystal volume

fractions between 40 and 70 vol%, this mechanism allows gas permeability to reach the order of 10^{-10} m^2 , which is two to five orders of magnitude higher than permeability calculated for bubbles alone at an equivalent porosity (Klug and Cashman, 1996; Burgisser et al. 2017). Under such permeable conditions, it is much more plausible that magma succeeds to extensively degas and outgas, even at the high pressures and low gas volume fractions typical of the deepest parts of a volcanic conduit. In addition, the formation of such channel-like porous pathways reduces significantly the percolation threshold, which is the critical vesicularity at which system-spanning bubble connectivity and permeability occur (Lindoo et al. 2017; Colombier et al. 2020). As a consequence, provided that crystallinity is high enough, outgassing can occur before or early during ascent, resulting in a magma column severely depleted in gas.

We revisited three data sets of the porosity distribution within volcanic conduits filled by andesitic magmas. They are from a Vulcanian explosion on February 11, 2010 at Soufrière Hills volcano, Montserrat (Burgisser et al. 2019), an explosive event on October 26, 2010 at Merapi volcano, Indonesia (Drignon et al. 2016), and a large Vulcanian event that occurred on July 14, 2013 at Tungurahua volcano, Ecuador (Gaunt et al. 2020). We show that the magmas feeding these Vulcanian events were sufficiently crystal rich to promote highly efficient outgassing by channelling.

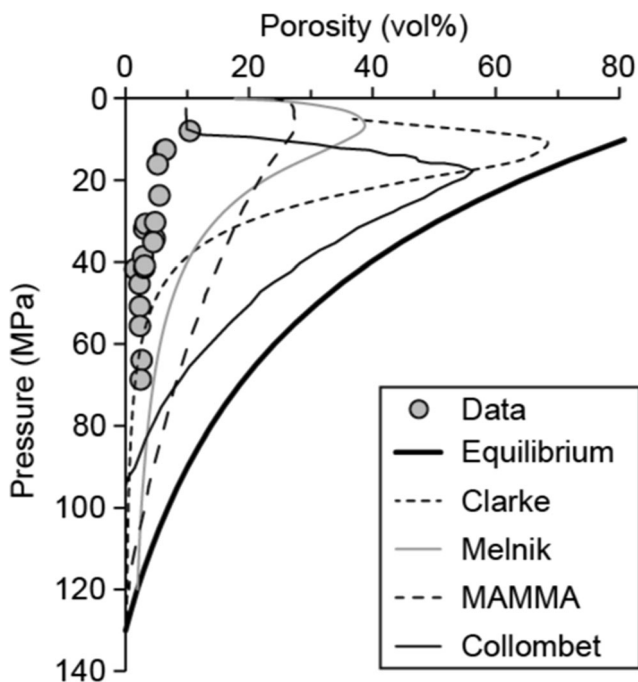


Fig. 1 Porosity as a function of pre-explosive pressure for the February 10, 2010 Vulcanian explosion at Soufrière Hills. Data are from Burgisser et al. (2019) and the «equilibrium» curve corresponds to closed-system degassing. Other curves are from the open-system degassing conduit flow models of Clarke et al. (2007), Melnik and Sparks (2002), the MAMMA code (La Spina et al. 2017; Degruyter et al. 2012), and Collombet (2009)

Geological context

The ongoing eruption of Soufrière Hills is dominated by lava dome effusion with intermittent collapse. The magma emitted is andesitic in bulk composition with a rhyolitic melt. The fifth phase of lava extrusion since the beginning of the eruption was marked by a succession of dome growth as lava lobes and spines followed by partial dome collapse (Wadge et al. 2014; Cole et al. 2014). The February 11, 2010 explosion was preceded by two small Vulcanian events on February 5 and 8 (Stinton et al. 2014; Cole et al. 2015). The February 11 event was mostly likely triggered by a dome collapse that started 1 h and 27 min prior to the onset of the Vulcanian explosion. Burgisser et al. (2019) analyzed twenty-three samples of the resulting pumice-rich, pyroclastic density current deposits, and pumice fallout deposits. Phenocrysts are mostly plagioclases that are up to 5 mm across (Higgins and Roberge, 2003). Large plagioclases have irregular shapes and smaller plagioclases are euhedral. Euhedral amphiboles up to 12 mm across are also present with a low number density. Microlites are mostly plagioclases with a concave up distribution in the 20–1000 μm^2 range when the log of the number density in mm^{-2} is plotted against crystal area (Couch et al. 2003) and short/long axis ratios of ~0.5 (Murch and Cole, 2019).

Merapi volcano produced in 2010 the largest explosive eruption since 1872 (Surono et al. 2012). This unusual event, which emitted basaltic andesites with a rhyolitic melt (Costa et al. 2013), occurred in several stages between October 26 and November 23 (Komorowski et al. 2013; Jenkins et al. 2013). The first large explosion lasted for 2 h on October 26, producing an ash plume and pyroclastic density currents. This explosion had a phreatomagmatic component and was interpreted as a laterally directed explosion from a newly formed cryptodome. Drignon et al. (2016) analyzed forty-one samples from a pumice levee of the valley-filling pyroclastic deposits produced by the October 26 event. Phenocrysts populations vary little between the recent eruptions (van der Zwan et al. 2013). Crystals that are 1.6–4 mm across make up one population with a size distribution that is approximately a straight line when the log of the number density in mm^{-4} is plotted against crystal size. The most common phenocrysts are plagioclases and pyroxenes that both have subhedral morphologies with evidences of resorption (Erdmann et al. 2016). Microlites are mostly plagioclases with a rectangular prism habit, areas of 10–15 μm^2 , and short/long axis ratios ranging from 0.35 to 0.67 (Costa et al. 2013).

The latest activity (1999–2016) at Tungurahua volcano varied from small-scale gas and ash venting and Strombolian outbursts to rare sub-Plinian events (Eychenne et al. 2012; Hall et al. 2015; Battaglia et al. 2019). The magma emitted is a low silica andesite with a high silica andesitic melt. The last 6 years of this eruptive phase was marked by two to three months of relative quiescence followed by Vulcanian events and ending with several weeks of low-explosivity Strombolian activity and ash venting (Hidalgo et al. 2015). On July 14, 2013, an unusually large Vulcanian event occurred at 06 h 46 (local time), producing a large ash column and pyroclastic density currents that travelled up to 7.5 km away from the vent. Gaunt et al. (2020) analyzed twenty-seven samples from three lithological groups (pyroclastic current deposits, fallout pumice, and ballistic ejecta) present in the ejecta. Plagioclase is the most abundant phenocryst phase, followed by pyroxene (Samaniego et al. 2011). Both exhibit mostly euhedral habits. Microlites are mostly plagioclase with habits ranging from rectangular prisms to acicular crystals (Gaunt et al. 2020). Dense plug rocks have mean microlite areas of 4.2–26 μm^2 with mostly tabular morphologies. Juvenile vesicular clasts of the pyroclastic current deposits have mean microlite areas of 10–66 μm^2 with occasional swallow-tail and hopper morphologies.

Methods

We modified data treatment of the recompression model of Burgisser et al. (2010) used by Drignon et al. (2016), Burgisser et al. (2019), and Gaunt et al. (2020). We briefly outline the

data acquisition and the data treatment done in these three studies before describing our modification. The petrological and textural analysis of the samples was carried out in the three studies according to the procedures outlined in Burgisser et al. (2010) and Drignon et al. (2016). Polished sections were imaged by scanning electron microscopy (SEM) or by element mapping based on energy-dispersive spectroscopy (EDS). Images were taken at several magnifications depending on the average size of the vesicles and crystals. Images were used to quantify the amounts of vesicles, glass, phenocrysts, and microlites in the samples by manually tracing each of the elements (SEM) or by automatic thresholding and by successive subtractions of Boolean combinations of the binary images of the analyzed elements (EDS). The segmented images were then used to measure the proportions of phenocrysts, microlites, and vesicles. In this study, we use “vesicles” and “vesicularity” to characterize voids regardless of genesis. We use “bubbles” and “porosity” to characterize voids resulting from the exsolution of magmatic volatiles.

Imaged vesicles were subdivided in four types (Fig. 2, Burgisser et al. 2010; Giachetti et al. 2010). The first type was composed of large, deformed vesicles of equivalent diameter $>300 \mu\text{m}$ and circularity <0.2 . The second type was composed of small, rounded vesicles of equivalent diameter $<40 \mu\text{m}$ and circularity >0.65 . The third type was composed of large angular voids between crystal fragments and of irregular voids delimited by crystal faces that are found in dense, diktytaxitic samples. The last type was composed of the remaining vesicles, which are of intermediate sizes and often composed of coalesced bubbles. Type 1 vesicles were caused by degassing during magma ascent from the reservoir. The sudden decompression linked to the explosion nucleated new, syn-explosive bubbles (Giachetti et al. 2010). The first syn-explosive bubbles are of Type 4 because they had enough time to grow and coalesce before quenching. The latest syn-explosive bubbles are of Type 2 because they were quenched as small, isolated vesicles. Finally, Type 3 vesicles that are gaps between crystal fragments (e.g., Fig. 7 in Giachetti et al. 2010; Costa et al. 2013; Fig. 1a in Burgisser et al. 2019) result from crystal failure caused by the decompression accompanying conduit evacuation (Burgisser et al. 2010; Giachetti et al. 2010; Burgisser et al. 2019). The remaining Type 3 vesicles found in diktytaxitic samples are likely due to reorganization of voids under shear (Laumonier et al. 2011).

The recompression model of Burgisser et al. (2010) assumes that, prior to explosion, the piece of magma to be ejected is at a pressure P_i and porosity, ϕ , with water weight fraction distributed as exsolved, x_i , and dissolved, s_i . The clast is quenched at pressure P_q , porosity ϕ_q , and dissolved water content, s_q . Quench porosity, ϕ_q , is the sum of volume fractions of the four vesicle types. Only Type 1 vesicles were present in the conduit prior to the explosion. Type 2 vesicle nucleate during the explosion but were not affected by outgassing. Type 3 and

4 vesicles both appeared during the explosion and could participate in outgassing because they feature various degrees of interconnection (Giachetti et al. 2010). The weight fraction of the exsolved water content at quench time is thus composed of an outgassed part, x_{out} , and a part remaining within the clast that is divided into three weight fractions: x_{q1} (Type 1 vesicles), x_{d1} (Type 2 vesicles), and x_{q2} (Type 3 and 4 vesicles). Similarly, quench pressures differ from pre-explosive pressures; they are at least equal to atmospheric pressure and at most equal to the pressure differential that clasts can sustain before breaking (see below). The conversion from quench to pre-explosive conditions (Fig. 2) was done by a mass balance linking the state of the magma just before the explosive event (pre-explosive state characterized by P_i , ϕ , s_i and x_i) to that once the magma has quenched (quench state characterized by P_q , ϕ_q , s_q , x_{q1} , x_{d1} , and x_{q2}).

Model input data are the magma temperature, the densities of melt and crystals at that temperature, ϕ_q , and, to obtain P_i , one of plagioclase microlite content, or glass water content. In Gaunt et al. (2020), P_i was obtained by converting the glass-referenced volume proportions of plagioclase microlites of each sample into pressure. In Drignon et al. (2016) and Burgisser et al. (2019), P_i was calculated by using the glass water content determined by elemental analyzer and converting successively glass water content into dissolved water content and into pressure with a solubility relationship. The original recompression model has four free parameters (Burgisser et al. 2010). The first one, $O = x_{out}/(x_{q1} + x_{q2} + x_{d1} + x_{out})$, quantifies the gas fraction outgassed during the explosion to propel the ejecta. This poorly constrained parameter, which has a modest effect on pre-explosive values (Burgisser et al. 2010), is assumed to lie between 10% and 70–82% with a reference value of 50%. The second parameter, H , estimates the maximum, near-instant pressure drop that clasts can sustain before breaking (Mueller et al. 2008) as a proxy for quench pressure. In other words, P_q is the smallest of P_i and $P_{atm} + H P_{Mueller}$, where P_{atm} is the atmospheric pressure, $P_{Mueller}$ is the value of the pressure drop, and H is a multiplicative factor that was assumed to lie between 0.5 and 2 with a typical value of 1. The upper limits of O and H were chosen so that the maximum total water content of every clast lies below that inferred in the reservoir and that all clasts undergo syn-explosive inflation so as to match textural observations. The upper values of O were 70, 76, and 82% for Tungurahua, Soufrière Hills, and Merapi, respectively. The two last parameters of the model quantify the proportions of vesicles: $E = (x_{d1} + x_{q2})/x_{q1}$ and $F = x_{d1}/x_{q1}$. As vesicle types occur in similar proportions in the products of a given explosion, Burgisser et al. (2010) and the authors of the three data sets studied herein (Drignon et al. 2016; Burgisser et al. 2019; Gaunt et al. 2020) used a lumped

approach; they averaged vesicle proportions in all samples of a given explosion. They then calculated E and F using the median proportions and standard deviations of each vesicle type.

In this study, we attempted to gain precision in the pre-explosive porosities by considering for each clast the respective proportions of the vesicle types. These proportions were published in the original studies. Using individual vesicle proportions means that E and F were no longer considered as free parameters with a median value and a standard deviation. Instead, they were considered as input parameters with an assumed negligible uncertainty, which reduced the number of degrees of freedom of the recompression procedure from four to two. In the Drignon et al. (2016) study of the October 26 event at Merapi, for instance, the vesicles of Types 1, 2, and 3–4 were present in respective median proportions of 28.4:2.5:70, which yields $E=2.7$ and $F=0.14$. We replaced these median proportions by the individual values of each sample (AME 10 A1: 33.5:3.1:63.4, etc.) to obtain E and F values for each sample. Beyond reducing the number of sources of uncertainties, this modification evidenced a shortcoming of the vesicle size distribution analysis (some samples were imaged at a resolution insufficient to correctly discriminate pre- from syn-explosive vesicles in the range 40–200 μm , Supplementary Text S1), which led us to discard data from Drignon et al. (2016).

The recompression model has two types of uncertainty. Analytical uncertainties result from error propagation of the uncertainties on quench vesicularities, glass water contents, and plagioclase microlite proportions. Analytical uncertainties for each sample were calculated with four sets of model outputs that used the reference values of H and O and the respective minimum and maximum values of ϕ , microlite content and/or glass water content. Analytical errors on pre-explosive porosity are small in absolute value (<1 vol%). Our new procedure with fewer free parameters does not significantly affect these absolute errors (<15%). Similarly, errors on pre-explosive pressure are modified by <10% and typically by <2%. These changes will not be discussed further as they are smaller than those stemming from model uncertainties. This second type of uncertainty results from propagation of the uncertainties on H and O . The reference values and bounds of these two parameters were combined to yield five sets of pre-explosive pressures and porosities. The set with the reference values was kept as the average set and the two sets with the largest and smallest porosity values at any pressure were kept as extrema to characterize model uncertainty. Only these three sets are reported in the “Results” section.

In the case of a rigid crystal network with crystal volume fraction ϕ_x between 0.4 and 0.7, the minimum porosity required to make percolation possible (i.e., the percolation

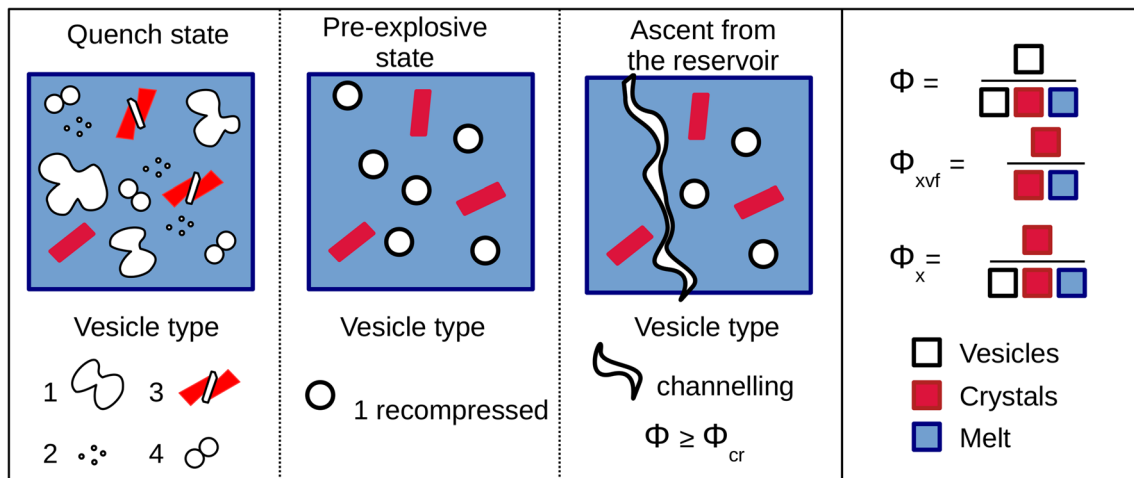


Fig. 2 Schematic depiction of the textural elements considered. Clasts represent the magma in “Quench state”, which is composed of melt (blue), crystals (red), and vesicles (white). Vesicles are pre-explosive (Type 1), syn-explosive and isolated (Type 2), syn-explosive gaps between broken crystals (Type 3), and syn-explosive and coalesced (Type 4). Prior to ejection, the magma is in a “Pre-explosive state.” It is composed of Type 1 vesicles that occupy a smaller volume than in the

threshold), ϕ_{cr} (Fig. 2), has been modelled as a third-degree polynomial equation:

$$\phi_{cr} = a\phi_x^3 - b\phi_x^2 + c\phi_x + d \tag{1}$$

where the constants are $a=0.7495$, $b=0.4268$, $c = -0.1626$, and $d=0.1478$ for Degruyter et al. (2019) or $a=2.75$, $b=2.79$, $c=0.6345$, and $d=0.0997$ for Parmigiani et al. (2017). The difference between these two sets of constants is due to the initial conditions chosen for the bubbles. In the case of Parmigiani et al. (2017), the initial positions of the bubbles and their respective size were set randomly, whereas these parameters followed a spinodal distribution in the case of Degruyter et al. (2019). A spinodal distribution means that the size and the position of bubbles satisfy the principle of mass conservation and capillary stresses, which leads to more consistent and more accurate initial conditions. This higher level of physical verisimilitude led us to use the set of parameters of Degruyter et al. (2019).

The vesicle-free crystal content, ϕ_{xvf} , is related to ϕ_x by (Fig. 2):

$$\phi_x = (1-\phi)\phi_{xvf} \tag{2}$$

Drignon et al. (2016) reported bulk volume fractions of vesicles, phenocrysts and microlites, from which ϕ_{xvf} (Table 1) was calculated using Eq (2). Burgisser et al. (2019) reported ϕ_q and ϕ_{xvf} . We used their original unpublished quantifications of microlites to obtain vesicle-free volume fractions of phenocrysts. Gaunt et al. (2020) reported bulk volume fractions of vesicles, of plagioclase and pyroxene phenocrysts, and of plagioclase and pyroxene microlites. We

used their original unpublished quantifications of oxide phenocrysts and microlites to calculate ϕ_{xvf} . For a given vesicle-free crystal content, there is one critical porosity such that $\phi=\phi_{cr}$:

$$a(1-\phi)^3\phi_{xvf}^3 - b(1-\phi)^2\phi_{xvf}^2 + c(1-\phi)\phi_{xvf} + d - \phi = 0 \tag{3}$$

For each ϕ_{xvf} within the 40–70% interval, we solve equation (3) to obtain a solution $\phi_{cr}=f(\phi_{xvf})$. The associated uncertainties, $d\phi_{xvf}$, were obtained by error propagation and mostly reflect natural variability. Uncertainties on the critical porosity, $d\phi_{cr}$, were calculated using the variation of the f function: $d\phi_{cr}=df(d\phi_{xvf})$.

Results

Considering the vesicle proportions of each sample instead of an average value does not change much (<17%) the final values of pre-explosive pressures (Fig. S1). When using microlites (Gaunt et al. 2020), no pressure change occurs because the power-law relationship linking microlite proportion to pressure does not depend on vesicle content. Pre-explosive porosities are more influenced by this reduction of free parameters. Samples located at pressures >10 MPa change by <10% from the original value. Shallower samples undergo porosity changes of up to 25% with one outlier at 40% (Fig. S2), but the general trend with pressure remains (Fig. S1). Changes in model uncertainties compared to the ones from the original studies are small but uneven between data points, varying by <15% from the original value except for a couple of samples

Table 1 Pre-explosive volatile proportions, vesicle-free crystal proportions, and pressures. Values in parenthesis are relative uncertainties in % except for the pressure, where they indicate lower and upper bounds of uncertainties in MPa. Uncertainties on phenocryst content are sometimes very low (<1%), which reflects that few SEM

images were imaged to characterize phenocrysts. Uncertainties on the total crystal fraction include those due to microlite, which are obtained from a larger number of images. They thus reflect more accurately the natural spatial variability

	Pressure (MPa)	Porosity ^a (vol%)	Gas ^b (ppmw)	Phenocrysts (vol%)	Crystals (vol%)
Soufrière Hills					
AMO 210 A	40 (-9, +10)	1.9 (1)	0.6	34 (2)	54 (10)
AMO 210 C	51 (-25, +31)	2.3 (2)	0.92	34 (12)	55 (22)
AMO 210 D	14 (-3, +3)	1.9 (1)	0.2	31 (6)	39 (11)
AMO 210 E	54 (-19,+22)	3.5 (0)	1.54	48 (0.3)	69 (9)
AMO 210 F	33 (-8, +9)	1.6 (1)	0.41	50 (2)	66 (13)
AMO 210 G	42 (-13, +15)	1.2 (3)	0.39	40 (12)	63 (11)
AMO 210 H	12 (-5, +6)	8.5 (1)	0.89	39 (8)	65 (12)
AMO 210 L	46 (-13, +14)	1.4 (2)	0.52	59 (3)	77 (6)
AMO 210 Q	41 (-7, +7)	3.4 (1)	1.14	32 (1.3)	40 (14)
WP1.095A	24 (-5, +5)	4.3 (0)	0.86	24 (0.4)	52 (3)
WP1.095B	16 (-6, +7)	7.2 (0)	0.95	32 (0.2)	59 (9)
WP1.108A	31 (-5, +5)	2.8 (0)	0.72	32 (0.3)	52 (10)
WP1.108B	56 (-5, +5)	7.8 (1)	3.68	36 (1.1)	48 (3)
WP2.200A	36 (-8, +9)	2.8 (0)	0.81	42 (0.3)	63 (19)
WP2.200B	31 (-2, +2)	3 (0)	0.76	31 (0.7)	42 (3)
WP2.201A	35 (-8, +9)	4.6 (0)	1.33	45 (0.2)	59 (10)
WP2.201B	69 (-14, +15)	2.4 (0)	1.36	31 (0.2)	51 (8)
WP2.329A	7 (-1, +1)	23.6 (0)	1.62	11 (1.2)	27 (15)
WP2.329B	41 (-4, +4)	2.7 (1)	0.89	51 (2)	65 (3)
Merapi Oct. 26					
AME 10 A1	75 (-22, +25)	2.3 (4)	1.27	33 (7)	70 (11)
AME 10 A2	100 (-34, +38)	1.5 (4)	1.12	44 (8)	79 (8)
AME 10 A3	150 (-123, +174)	1.2 (3)	1.32	40 (3)	82 (11)
AME 10 A4	100 (-22, +24)	1.6 (5)	1.16	45 (8)	80 (8)
AME 10 A5	73 (-25, +29)	2.4 (3)	1.32	47 (5)	76 (6)
AME 10 A6	58 (-12, +13)	3.1 (2)	1.32	46 (3)	72 (5)
AME 10 B1	158 (-48, +53)	0.9 (4)	1.03	41 (9)	80 (10)
AME 10 B2	63 (-11, +12)	2.3 (3)	1.05	50 (5)	72 (8)
AME 10 B4	268 (-106, +118)	0.6 (4)	1.14	36 (6)	87 (6)
AME 10 B5	260 (-153, +184)	0.4 (5)	0.73	44 (13)	87 (12)
AME 10 C1	159 (-57, +64)	1 (1)	1.13	38 (1)	80 (14)
AME 10 C2	141 (-31, +33)	0.7 (2)	0.69	38 (5)	81 (6)
AME 10 C3	55 (-17, +20)	2.8 (2)	1.16	46 (3)	70 (10)
AME 10 C4	77 (-24, +27)	1.4 (3)	0.78	44 (7)	77 (7)
AME 10 D1	107 (-25, +27)	1.1 (3)	0.88	44 (4)	79 (9)
AME 10 D2	85 (-37,+43)	1.4 (5)	0.88	42 (11)	79 (11)
AME 10 D3	64 (-37, +47)	2 (8)	0.96	34 (20)	69 (27)
AME 10 D4	63 (-14, +15)	2.8 (5)	1.34	42 (12)	71 (10)
AME 10 E1	75 (-23, +26)	1.2 (2)	0.67	42 (6)	74 (11)
AME 10 E2	202 (-67, +74)	0.9 (4)	1.26	57 (4)	88 (4)
AME 10 E3	59 (-11, +12)	2 (3)	0.86	43 (9)	74 (8)
AME 10 E4	77 (-15, +16)	1.9 (5)	1.1	45 (10)	72 (8)
AME 10 E5	227 (-78, +87)	0.5 (4)	0.85	45 (12)	86 (11)
AME 10 F1	12 (-5,+5)	2.3 (20)	0.2	21 (23)	54 (17)

Table 1 (continued)

	Pressure (MPa)	Porosity ^a (vol%)	Gas ^b (ppmw)	Phenocrysts (vol%)	Crystals (vol%)
AME 10 G1	42 (-16, +18)	2.3 (2)	0.76	52 (5)	75 (7)
AME 10 G2	75 (-54, +75)	1.1 (2)	0.78	51 (6)	82 (11)
AME 10 G3	44 (-21, +25)	0.3 (15)	0.48	41 (9)	70 (12)
AME 10 GA	94 (-25, +28)	2.8 (1)	0.89	48 (10)	81 (9)
AME 10 GB	196 (-80, +92)	1.6 (1)	0.86	47 (8)	88 (8)
Tungurahua					
1	0.8 (-0.2, +0.4)	36.8 (3)	0.33	15 (21)	55 (12)
2	0.5 (-0.1, +0.1)	0 (8)	0	46 (10)	73 (9)
4	0.9 (-0.2, +0.3)	0.9 (11)	0.01	42 (14)	67 (13)
6	0.5 (-0.1, +0.2)	0.3 (30)	0.001	39 (36)	70 (32)
7.5	0.6 (-0.2, +0.3)	0.8 (9)	0.004	30 (12)	62 (12)
11	3 (-1, +1)	0 (1)	0	25 (1.4)	44 (5)
12	109 (-63, +91)	0.3 (1)	0.24	34 (0.8)	38 (5)
13	5 (-2, +9)	44.2 (1)	2.53	32 (2)	48 (14)
14	31 (-17, +68)	8.5 (4)	2.07	38 (4)	45 (6)
16	1.6 (-0.4, +0.5)	15.7 (4)	0.21	31 (3)	55 (5)
17	24 (-8, +16)	1.7 (2)	0.29	36 (6)	43 (6)
18	34 (-15, +41)	6.1 (1)	1.57	34 (2)	43 (6)
20	66 (-14, +20)	1.5 (2)	0.69	31 (3)	36 (4)
21	5 (-3, +8)	3.2 (2)	0.12	36 (3)	51 (10)
22	2 (-1, +5)	0 (4)	0	26 (3)	48 (15)
26	51 (-36, +149)	8 (3)	3.14	32 (2)	39 (9)
27	15 (-5, +10)	8.5 (3)	1.01	34 (5)	42 (8)
28	5 (-2, +9)	36.5 (3)	1.86	29 (6)	45 (12)
29	30 (-17, +82)	7.7 (1)	1.77	30 (0.8)	36 (6)
30	4 (-1, +2)	51.7 (1)	3.14	23 (4)	41 (8)
34	1.2 (-0.3, +0.4)	45 (3)	0.69	25 (2)	53 (6)
35	4 (-1, +2)	11.5 (3)	0.4	28 (3)	46 (5)
36	5 (-1, +2)	8.1 (1)	0.33	30 (2)	47 (7)
38	31 (-14, +38)	10.6 (1)	2.62	39 (2)	45 (4)
39	31 (-17, +67)	1.5 (2)	0.33	34 (5)	40 (7)
40	10 (-0.1, +0.1)	25.7 (2)	2.43	38 (2)	49 (2)
41	174 (-79, +26)	0.3 (2)	0.4	26 (3)	32 (4)

with vanishing porosity. As a result, the overall respective envelopes of model uncertainties are similar for each volcano.

Two conditions need to be met for outgassing to occur by channelling (Parmigiani et al. 2017; Degruyter et al. 2019). The first condition is that total crystal content must be between 40 and 70 vol%. Provided the germane amount of crystals, the second condition is that a critical bulk porosity is reached. Channelling allows gas escape at very low gas volume fraction with a percolation threshold below 10 vol%. We used the critical values given by the empirical relationship of Degruyter et al. (2019) because they correspond to more realistic initial conditions, but similar results are found when using the Parmigiani et al. (2017) values. To take the empirical

nature of these fits into account, we also considered the maximum and minimum percolation values they yield within the validity bounds of crystal content (5 and 12 vol% porosity, respectively). Once channelling is established, outgassing rate is controlled by a balance between magma permeability, driving pressure, and the collapse rate of the medium. As a result, outgassing could evacuate more gas than the critical porosity if the crystal framework is mobile enough to collapse. Such hysteresis has been proposed to occur at low (Rust and Cashman, 2004; Michaut et al. 2009; Gonnermann et al. 2017) and high crystal contents (Colombier et al. 2020), albeit not by channelling because of its inherent assumption of rigid crystal framework. In the absence of more specific evidence,

we considered that non-vanishing porosities lower than the percolation threshold could result from channel collapse.

To test if channelling could explain low porosity distributions within volcanic conduits before explosion, we assessed to which extent these two conditions of crystallinity and porosity were met in three sets of data on andesitic products from different volcanoes. These datasets are composed of the pressures associated with the corresponding pre-eruptive porosities and of the amounts of phenocrysts (which are generally already present in the magmatic chamber) and microlites (which develop during magma ascent). It is important to consider these two populations of crystals since they could, depending on how their amounts change during ascent, prevent or enhance channelling.

Montserrat

The amounts of “phenocrysts” and “phenocrysts plus microlites” in the Soufrière Hills samples from 2010 are plotted in Fig. 3a. Phenocrysts were first present in the magma chamber and their amount is generally lower than 40%, which is not compatible with channelling. Then, microlite crystallization occurs during magma ascent, increasing the total amount of crystals from 30 vol% to approximately 55 vol% on average, thereby helping channelling and thus outgassing to develop. Figure 3b shows pre-explosive porosities of the samples, of closed-system degassing, and of the channelling threshold. All threshold porosities are within a narrow range smaller than 5 vol%. Considering that all samples have a porosity well below that of closed-system degassing, it means that most of the gas present in the conduit

has been lost. Physical conditions propitious to channelling were thus probably met during ascent. However, it appears that most measured porosities are slightly below the threshold values, except two points among the shallowest samples and one point around 57 MPa that are slightly above threshold. This situation indicates that, if channelling occurred, a little more than the gas in excess of the threshold value has been lost, deflating the magma back below the critical porosity.

Merapi

Data from the October 26, 2010 Merapi eruption are particularly interesting because they provide information down to ~10 km (270 MPa), which is close to the pure water exsolution level for that eruption (Erdmann et al. 2016; Drignon et al. 2016). Estimating the exsolution level at Merapi is a complex task because (1) a significant amount of CO₂ coexisted with H₂O in the gas phase and (2) the magmas feeding the 2010 eruption were stored at multiple levels and mixed prior to their final ascent towards the surface (Costa et al. 2013; Nadeau et al. 2013; Preece et al. 2014; Erdmann et al. 2016; Widiyantoro et al. 2018). The mixing process started by magma assembly at depth and continued during ascent. This induced complexities in the crystal cargo that hinders straightforward interpretations of porosity and crystal contents (Supplementary Text S2). Here, we framed the likely conduit conditions according to the experimental results of Erdmann et al. (2016) by performing two closed-system, multicomponent decompressions. Following Drignon et al. (2016), we used the model D-Compress (Burgisser et al. 2015) to simulate the porosity evolution of rhyolitic melts undergoing

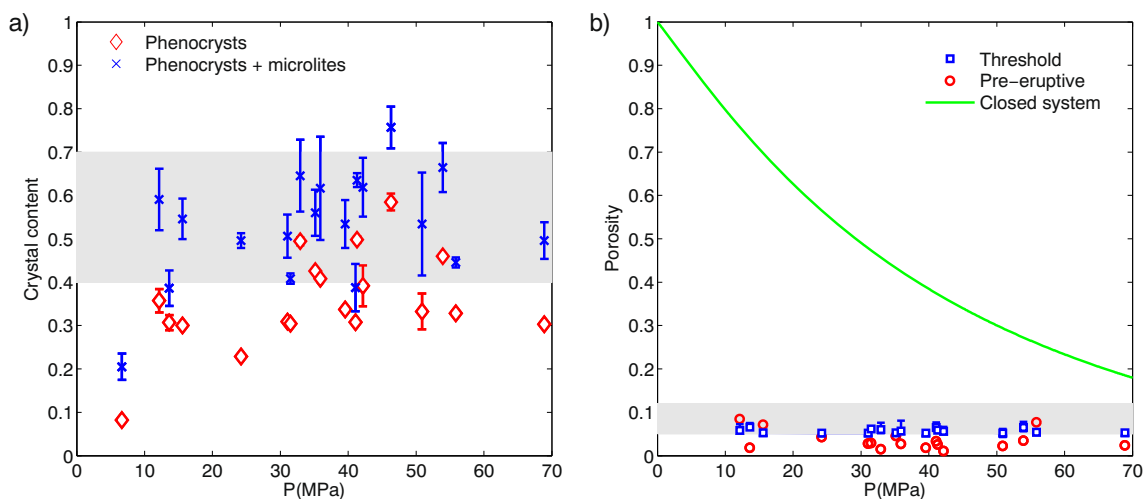


Fig. 3 **a** Amount of phenocrysts (red) and phenocrysts plus microlites (blue) relative to pressure for Soufrière Hills according to Burgisser et al. (2019). The shaded region covers the validity domain for the development of channelling according to Parmigiani et al. (2017). **b** Porosity thresholds calculated from Degruyter et al. (2019) and

associated uncertainties (blue) for Soufrière Hills. Samples with crystal contents outside the validity range were discarded. Red dots are observed porosities. The associated uncertainties are smaller than the symbols. The green line gives theoretical porosities for a closed system. The shaded region covers the extreme porosity threshold values

isothermal, equilibrium decompression at NNO+1. The first decompression represents the hotter recharge magma at 975 °C. It starts from 250 MPa with 5 wt% melt H₂O content and 400 ppm melt CO₂ content, which yields a CO₂/H₂O molar ratio of 0.2. The second represents the colder resident magma at 925 °C. It starts from 175 MPa with 3 wt% melt H₂O content and 500 ppm melt CO₂ content, which yields a CO₂/H₂O molar ratio of 0.66. The resident and recharge magmas were mixed in a way that we expect to fall within these two end members. The initial porosity is mostly unconstrained, so we considered a small (\ll 1 vol%) and a large (10 vol%) value for each magma.

Figure 4a shows the phenocrysts and total crystal content for Merapi conduit prior to the October 26 explosion. Unlike at Soufrière Hills, phenocrysts alone are already within the range for which channelling is possible. The amount of crystals already present in reservoir(s) was thus sufficient to foster outgassing at depth without magma ascent if sufficient gas was present. There was also enough time for the awakened reservoir to degas during the weeks to months prior to eruption (Budi-Santoso et al. 2013). If microlites are taken into account, however, the total crystal content clearly rises above 70 vol% in most of the magmatic column. Thus, if outgassing occurred by channelling, this outgassing mechanism took place earlier or during the first phase of microlite crystallization. As numerically established by Parmigiani et al. (2017) and Degruyter et al. (2019), once 70 vol% of crystals was reached, channelling mostly likely stopped.

Pre-eruptive porosities, percolation thresholds, and associated uncertainties are shown in Fig. 4b. Above ~70 MPa, samples suggest that the conduit was filled with nearly gas-free magma, well below percolation threshold. This

observation makes the two scenarios starting with high initial porosities unlikely, so they were not given further consideration. Assuming that the porosity evolution was controlled by an initially gas-poor recharge magma, no bubbles are expected at pressures higher than 250 MPa, which is consistent with the very small values (<1 vol%) of the samples located around that pressure. At ~150 MPa, the gas available by closed-system degassing matches that needed for channelling (black line on Fig. 4b) although measured porosities are well below percolation. Assuming instead that the eruptive products sampled the resident magma brings the pressure at which closed-system porosities are within the threshold range from 150 to 70 MPa (green line on Fig. 4b). This situation is compatible with the vanishing measured porosities at higher pressure and the fact that porosities increase below 70 MPa while remaining below the threshold porosities.

The combined data of Fig. 4a and b suggest that deeper than 3 km (70 MPa), there was not enough gas available in the reservoir to be outgassed despite the favorable phenocryst content for channelling. Between 3 km and the surface, however, gas contents stemming from closed-system degassing would have been high enough for outgassing to occur. Shallower than 3 km, crystal contents vary from 40–50 vol% before microlite crystallization, to more than 70 vol% post-crystallization. If the shallow magma column stagnated while (or before) microlite crystallization occurred, channelling could have started before microlite crystallization and continued until 70 vol% of crystals was reached. If the magma still contained substantial gas volume fraction once this high limit of crystallinity reached, other mechanisms, such as cracks due to brittle failure of the melt, should be evoked to explain further outgassing. In any case, the

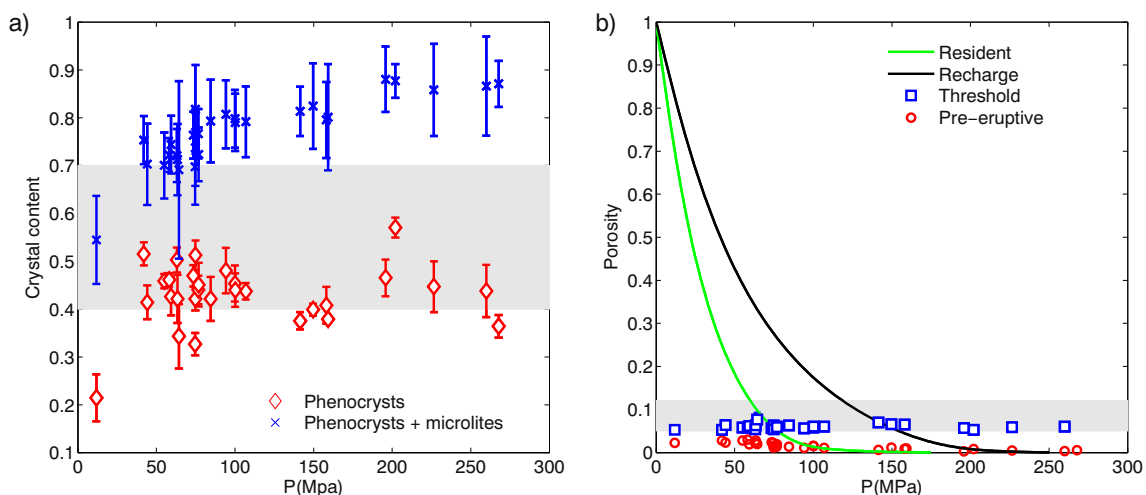


Fig. 4 **a** Contents of phenocrysts (red) and phenocrysts plus microlites (blue) as a function of pressure for Merapi according to Drignon et al. (2016). The shaded region covers the validity domain for the development of channelling according to Parmigiani et al. (2017). **b** Porosity thresholds calculated from Degruyter et al. (2019) and associated uncertainties (blue) for Merapi. Red dots are observed

porosities and the associated uncertainties are smaller than the symbols. Green and black lines give theoretical porosities for a closed system with 5 wt% H₂O and 400 ppm CO₂ in the melt (resident magma) and with 3 wt% H₂O and 500 ppm CO₂ in the melt (recharge magma) respectively. The shaded region covers the extreme porosity threshold values

degassing trends suggest that the analyzed clasts sampled the colder resident magma. As in the case of Soufrière Hills, pre-eruptive shallow samples display porosities below the critical threshold, possibly suggesting outgassing accompanied by deflating.

Tungurahua

Storage conditions at Tungurahua were more H₂O-rich than at Merapi, with a molar fraction of H₂O in the gas phase of 0.8 (Andújar et al. 2017). As a result, D-Compress runs with mixed H₂O-CO₂ fluids do not differ much from pure H₂O ones, and closed-system decompressions with pure water were assumed instead for simplicity. Porosities and crystal contents from Tungurahua give information from the surface down to ~7 km depth (170 MPa), which, like at Merapi, is deep enough to constrain the point at which gas loss starts. Similarly to Soufrière Hills, phenocrysts in the Tungurahua magma cannot trigger channelling alone (Fig. 5a). The total amount of crystals, however, approaches the lower limit of 40% around 100 MPa, and exceeds it for pressures lower than 50 MPa. This implies that microlites were required for channelling to occur possibly around 100 MPa, and more certainly around 50 MPa. Near the surface, the upper limit of 70% is overcome, stopping channelling and potentially fostering a shallow gas-rich area that appears clearly on the porosity data with values spanning from 25% to 50 vol% (Fig. 5b). Closed-system porosities suggest that gas was available for channelling at ~150 MPa, although the amount of crystals was not sufficient at this depth to foster channelling (Fig. 5a). The first calculated pre-eruptive porosity approaching the channelling threshold is located around 110 MPa and the first

pre-eruptive porosity which effectively coincides with that threshold appears at ~50 MPa (Fig. 5b). As a result, gas loss by channelling may have started between 110 and 50 MPa and was no longer possible below 10 MPa.

Discussion

Our data show that, to first order, channelling is a process that is consistent with the low porosities inferred in volcanic conduits prior to Vulcanian explosions. That channelling can occur during ascent due to an increase in crystal content brings a partial answer to the long-standing issue of gas transfer across the entire depth of magmatic systems (Oppenheimer et al. 2009) despite sometimes very high magma viscosity and no obvious physical mechanism of transfer (Edmonds et al. 2010). Gas percolation in magmas has long been studied in decompression experiments, which have notably shown that the presence of >20 vol% crystals lowers percolation thresholds compared to crystal-poor melts (Lindoo et al. 2017; deGraffenried et al. 2019). Such type of viscous percolation occurs when bubbles can expand spherically while pushing crystals apart (Colombier et al. 2020).

The percolation associated with channelling, on the other hand, is fostered by buoyancy-driven deformation of the bubbles in the constricted space between crystals and subsequent coalescence at moderate to low Bond numbers. Additional processes can also form similar channel-like interconnected porous pathways at low critical porosity in crystal-rich magmas. For instance, Colombier et al. (2020) showed that brittle-viscous coalescence (connectivity and formation of fracture-like chains of coalescing bubbles) is favored at melt viscosities higher than 10⁶ Pa.s and relatively high gas

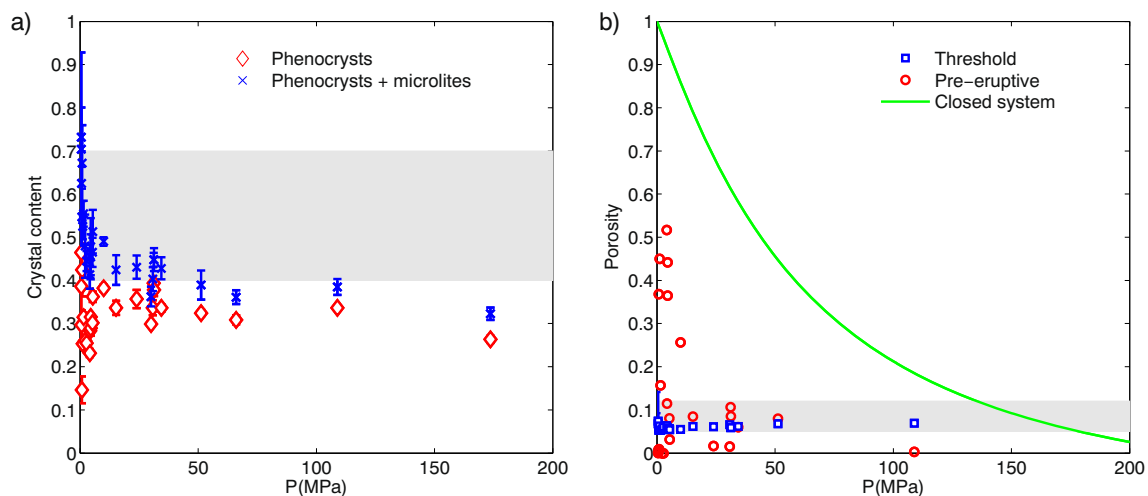


Fig. 5 **a** Contents of phenocrysts (red) and phenocrysts plus microlites (blue) as a function of pressure for Tungurahua according to Gaunt et al. (2020). The shaded region covers the validity domain for the development of channelling according to Parmigiani et al. (2017). **b** Porosity thresholds calculated from Degruyter et al. (2019) and

associated uncertainties (blue) for Tungurahua. Samples with crystal contents outside the validity range were discarded. Red dots are observed porosities and the associated uncertainties are smaller than the symbols. Green line gives the theoretical porosities for a closed system. The shaded region covers the extreme porosity threshold values

overpressure. Because of such alternatives, conditions adverse to channelling do not imply the absence of outgassing. Figure 6 shows a literature compilation of vesiculation experiments on crystal-free to crystal-rich magmas and magma analogues (Gardner et al. 2000; Larsen and Gardner 2000; Mangan and Sisson 2000; Gardner 2007; Takeuchi et al. 2009; Shea et al. 2010; Okumura et al. 2012; Martel and Iacono-Marziano 2015; Oppenheimer et al. 2015; Preuss et al. 2016; Colombier et al. 2020). Data is tallied in crystal-poor (<10 vol%), moderately crystal-rich (10–40 vol%), and crystal-rich (>50 vol%) categories, as well as whether samples underwent closed-system degassing, or bore connected bubbles networks able to outgas. Figure 6 suggests that experimental magma outgassing has only been explored in low-pressure, shallow conditions, which contrasts with our deep-seated determination of channelling during magma ascent. This compilation also confirms that high crystal contents promote outgassing at low percolation thresholds.

The conditions leading to channelling are based on several key assumptions (Parmigiani et al. 2017; Degruyter et al. 2019), the validity of which must be assessed in the case of conduit flow. One is that capillary forces dominate buoyancy forces so that the Bond number is 0.1–1. The Bond number depends on gravity, the density difference between melt and

gas, the surface tension, and the radius of the gas bubbles. A reasonable estimate for the melt density of the three studied volcanoes is 2300 kg/m^3 . According to Lyakhovskiy et al. (1996), surface tension can be taken as 0.05 N/m . The most variable quantity is bubble size because it depends highly on the pressure and bubble number density. A Bond number between 0.1 and 1 implies a bubble radius between 0.2 and 0.8 mm. At depth, bubbles that size and smaller were likely, and the assumption of dominating capillary forces holds. The possibility that bubbles adhere to crystal surfaces was also left aside. This is a reasonable assumption in conduit conditions because microlites are mostly composed of non-wetting phases like plagioclase in arc magmas. We note, however, that wetting phases like Fe-Mg silicates or Fe-Ti oxides are also present, which suggests that investigating how crystal adherence affects bubble channelling is a worthy pursuit.

Two other assumptions of Parmigiani et al. (2017) and Degruyter et al. (2019) are that the ambient pressure is lithostatic and that the crystal framework remains static during the onset of channelling. The lower crystallinity limit of 40 vol% stems from the assumption that crystalline matrix resists frictional sliding, which corresponds to a random loose packing. Their synthetic crystal size (between 3 and 5 mm) and shape distributions aim to represent a scaled version of phenocrysts prevailing in storage conditions (Crystal shapes are equant with aspect ratio ranging from 1 to 3, corresponding to plagioclase and pyroxene habitus with a narrow crystal size distribution). Microlite crystallization during ascent, however, yielded in our three studied cases linear to concave-up crystal size distributions with a significant proportion of highly elongated microlites. Random loose packing and frictional effects in such distributions occur at volume fraction lower than 40 vol%, possibility as low as 8 vol% (Saar et al. 2001; Guo et al. 2013). The bubble coalescence leading to channelling, however, is controlled by how much interstitial space occurs between crystals, which is inversely proportional to the cubic root of crystal volume fraction. It is thus unlikely that the onset of channelling occurs at crystallinities much lower than that proposed by Parmigiani et al. (2017), depending on crystal shapes and sizes. Similarly, the transition from channelling to bubble trapping could also occur at a different (yet probably close to) volume fraction than the 70 vol% determined numerically.

Bubble trapping assumes a static solid matrix. It is no longer static when either local overpressure occurs, or a far-field stress is applied to the medium, which are two likely processes in ascending magmas. Different regimes of matrix deformation by local gas overpressure exist. Analog experiments (Holtzman et al. 2012; Oppenheimer et al. 2015) show that a regime of slow solid matrix rearrangement occurs at the random loose packing, when gas bubbles begin to deform. This change is insensitive to liquid viscosity in the range 10–1000 Pa s. Another regime of rapid deformation of the

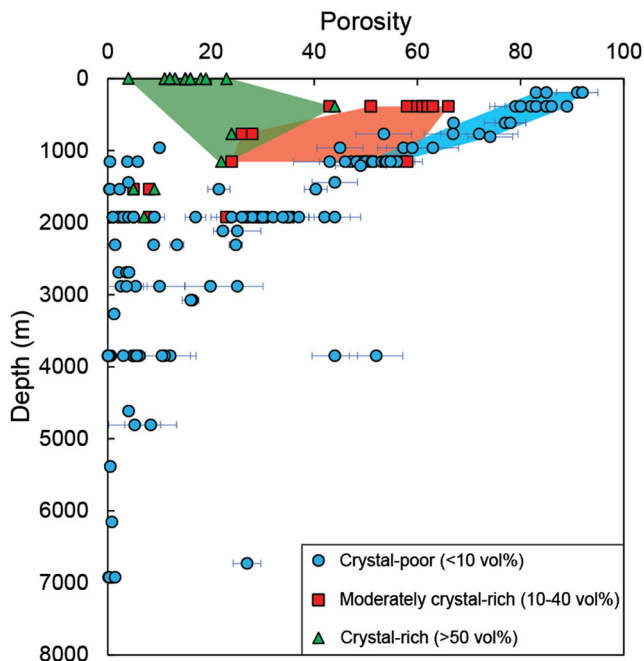


Fig. 6 Porosity profile as a function of depth for vesiculation experiments on crystal-free to crystal-rich magmas and magma analogues. The colored areas respectively overlap samples with connected bubbles networks capable of outgassing. All other samples featured closed system degassing. Data are from Gardner et al. (2000), Larsen and Gardner (2000), Mangan and Sisson (2000), Gardner (2007); Takeuchi et al. (2009), Shea et al. (2010), Okumura et al. (2012), Martel and Iacono-Marziano (2015), Oppenheimer et al. (2015), Preuss et al. (2016), and Colombier et al. (2020)

immersed granular medium by gas-induced overpressure has been described as “venting” (Varas et al. 2015) or “capillary fracturing” (Holtzman et al. 2012). It occurs near the random close packing (Oppenheimer et al. 2015), and it is characterized by gas migration in a fracture-like manner. These regimes have recently been proposed to play a role in Strombolian dynamics when gas proportions are large and melt viscosities low ($<5 \text{ Pa s}$; Barth et al. 2019; Oppenheimer et al. 2020). It is unclear yet probable that outgassing by channelling leads to limited grain displacement in melts of much higher viscosity. The two values of crystal content framing channelling are thus reasonable estimates that will be refined when reproduced experimentally with the assumption of static solid matrix relaxed. As the same reasoning holds for the critical porosity (Eq. (3)), the shaded regions in Figs. 3b, 4b, and 5b indicate the two extreme values ever reached by numerical simulations of channelling (Degruyter et al. 2019). Considering only these extreme values does not change the conclusion that conditions for channelling were met in the three studied cases.

Once channelling is established, gas evacuation can proceed to the point of fracture healing if large-scale stresses are applied (Caricchi et al. 2011; Laumonier et al. 2011; Heap et al. 2015). Such gas expulsion is thus expected in a crystal-rich magma sheared along a volcanic conduit (Thomas et al. 2019). Provided that Eq. (3) is accurate, this is the most probable explanation of the porosities close to but lower than the critical porosity at Soufrière Hills and Merapi (Figs. 3b and 4b). We reiterate that channelling in deforming crystal frameworks remains to be quantified to add weight to our inferences.

At Tungurahua, conditions for channelling were met between 110 MPa and a gas-rich region located at 1–10 MPa. Outgassing, however, could have happened through other mechanisms such as viscous percolation in the main part of the conduit owing to the low melt viscosity ($10^{3.7} \text{ Pa s}$ at the reservoir level, Chevrel et al. 2015), or brittle-viscous coalescence shallowly, where much higher melt viscosities are expected. Figure 7 shows closed-system degassing paths for three starting points: at 200 MPa (reservoir level, Andújar et al. 2017), at 108 MPa, and at 34 MPa. These intermediate pressures correspond to the samples closest to the points where total crystal contents reach and exceed the lower bound for channelling, respectively. The decompression starting at 108 MPa overestimates shallower porosities, whereas that starting at 34 MPa closely follows the trend of the most porous samples. That the measured shallow porosities can be explained by decompressing the residual porosity around 40 MPa suggests that gas loss by channelling was enabled by microlite crystallization between 100 and 40 MPa (1.6–2.9 km depth). The gas-rich region at 1–10 MPa (40–400 m depth) could be due to the ascent of material immediately below that was fast enough to minimize outgassing, or to gas accumulation. Accumulation

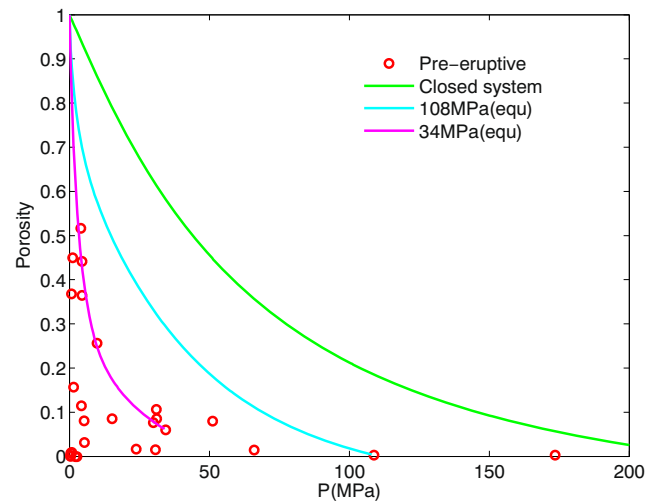


Fig. 7 Comparison at Tungurahua between pre-eruptive porosities (red circles), and theoretical porosities for closed systems starting decompressing at the reservoir level of 200 MPa (green line), at 108 MPa (cyan line), and at 34 MPa (magenta line)

implies that outgassing was inefficient close to the surface. This could be caused by a combination of hindered channelling at high crystal content, hindered brittle-viscous coalescence because of insufficient gas overpressure, and impermeable plug and conduit walls. Gas accumulation is supported by the near-surface observation that measured porosities decrease to very low values ($<1 \text{ vol\%}$), revealing the presence of a low permeability, rigid plug (Gaunt et al. 2020). Since the amount of crystals is very high in this plug, cracks or bubble connections (Heap et al. 2014) were not efficient enough to evacuate the residual gas, thereby allowing the gas-rich region to form.

Our results suggest that outgassing by channelling could have occurred down to (and probably deeper than) 2.7 km at Soufrière Hills, shallower than 3 km depth at Merapi, and between 1.5 and 3 km at Tungurahua. One implication of such widespread channelling depths is that, besides rapidly changing magma rheology to possibly trigger more explosive eruptions (Arzilli et al. 2019), microlites could also spur gas escape. Decompression-driven growth of phenocrysts (Befus and Andrews 2018) can also contribute to increase crystal volume fraction and foster channelling. Another implication is that outgassing by channelling could occur regardless of near-surface conditions such as the presence of a dome, a plug, or a permeable wallrock. Finally, the permeabilities reached by channelling are high for magmas in general, and several orders of magnitude higher than commonly admitted permeabilities at low porosity (Farquharson et al. 2015; Kushnir et al. 2016). Such high permeabilities would affect transitions in eruptive style (Cassidy et al. 2018), and the corresponding permeability relationships given by Parmigiani et al. (2017) and Degruyter et al. (2019) can readily be tested in conduit flow models.

Conclusions

We revisited three reconstructions of porosity and crystal distributions prior to Vulcanian events that occurred respectively on February 10, 2010, at Soufrière Hills volcano, Montserrat (Burgisser et al. 2019), on October 26, 2010, at Merapi volcano, Indonesia (Drignon et al. 2016), and on July 14, 2013, at Tungurahua volcano, Ecuador (Gaunt et al. 2020). They all feature porosities too low to be explained by common shallow processes such as connected bubble pathways or cracks. Our data show that these magmas have high enough crystal contents for outgassing to occur by a process named channelling. When the amount of crystals in a three-phase magma lies within the 40–70 vol% range, the interstitial space is narrow enough to force bubbles to form channels in which the gas buoyantly moves upwards but not so constricted that channel connections are ruptured (Parmigiani et al. 2017). Channelling creates gas permeability of the order of 10^{-10} m², which is two to five orders of magnitude higher than the other permeability processes at the equivalent bubble content.

At Soufrière Hills, microlite crystallization during ascent yielded conditions propitious to channelling from near surface down to a depth greater than 2.7 km. If confidence is given in the critical porosity quantification, outgassing deflated the magma slightly below the critical porosity, which suggests that large-scale stresses such as those related to conduit wall shearing were also at play in controlling the evolution of porosity during ascent.

At Merapi, the phenocrysts in the reservoirs could have fostered outgassing at depth without magma ascent. Closed-system degassing in response to ascent, however, only yielded enough gas for channelling at mid-conduit depths. The part of the conduit where both gas contents were large enough and calculated porosities fall within the percolation range is located around 3 km depth. In this region and in the shallower parts of the conduit, outgassing by channelling could have taken place during (and possibly before) microlite crystallization but before the 70% crystal content was reached. This suggests that the strong gas depletion in the magma column could have resulted from weak exsolution at the beginning of the ascent followed by channelling at depths shallower than 3 km. Of the two end-member magmas involved in the eruption that we considered in our analysis, this degassing behavior is best explained if the conduit was filled by the colder resident magma.

At Tungurahua, outgassing by channelling was enabled by microlite crystallization at 1.6–2.9 km depth. Near the surface, a low permeability plug trapped a gas-rich region between 40 and 400 m depth. Inefficient outgassing between 1.6 km and the gas accumulation region was

probably caused by a combination of hindered channelling at high crystal content, hindered brittle-viscous coalescence because of insufficient gas overpressure, and impermeable plug and conduit walls. This suggests that the triggering of the paroxysmal explosion was controlled by near-surface gas trapping.

We presented lines of evidence for deep gas loss prior to sudden explosive emissions of three basaltic andesitic to andesitic magmas. They suggest that channelling is a viable mechanism for gas to be removed from the magma column at various levels during ascent, yielding mostly gas-depleted magma columns prior to eruption. Such outgassing by channelling could thus influence eruptive style. Depending on the phenocryst content, microlite growth during ascent can either foster or impede gas escape by channelling. Considering the pervasive occurrence of microlites and ensuing high crystal contents in volcanic conduits, the high likelihood of outgassing by channelling implies that other outgassing mechanisms might not be as dominant as previously envisioned.

Supplementary Information The online version contains supplementary material available at <https://doi.org/10.1007/s00445-020-01433-0>.

Acknowledgments We thank Nicolas Gillet for the time spent to help with proper uncertainties calculations. We also thank the thoughtful and detailed comments of two anonymous reviewers and the constructive editorial handling of K. Cashman. This work was partially supported by the Agence Nationale pour la Recherche grant ANR-19-CE31-0007.

References

- Andújar J, Martel C, Pichavant M, Samaniego P, Scaillet B, Molina I (2017) Structure of the plumbing system at Tungurahua Volcano, Ecuador: insights from phase equilibrium experiments on July–August 2006 Eruption Products. *J Petrol* 58:1249–1278. <https://doi.org/10.1093/petrology/egx054>
- Arzilli F, La Spina G, Burton MR, Polacci M, Le Gall N, Hartley ME, Di Genova D, Cai B, Vo NT, Bamber EC, Nonni S, Atwood R, Llewellyn EW, Brooker RA, Mader HM, Lee PD (2019) Magma fragmentation in highly explosive basaltic eruptions induced by rapid crystallization. *Nat Geosci* 12:1023–1028. <https://doi.org/10.1038/s41561-019-0468-6>
- Barth A, Edmonds M, Woods A (2019) Valve-like dynamics of gas flow through a packed crystal mush and cyclic strombolian explosions. *Sci Rep* 9:821. <https://doi.org/10.1038/s41598-018-37013-8>
- Battaglia J, Hidalgo S, Bernard B, Steele A, Arellano S, Acuña K (2019) Autopsy of an eruptive phase of Tungurahua volcano (Ecuador) through coupling of seismo-acoustic and SO₂ recordings with ash characteristics. *Earth Planet Sci Lett* 511:223–232. <https://doi.org/10.1016/j.epsl.2019.01.042>
- Befus KS, Andrews BJ (2018) Crystal nucleation and growth produced by continuous decompression of Pinatubo magma. *Contrib Mineral Petrol* 173:92. <https://doi.org/10.1007/s00410-018-1519-5>

- Blower JB (2001) Factors controlling permeability-porosity relationships in magma. *Bull Volcanol* 63:497–504. <https://doi.org/10.1007/s004450100172>
- Budi-Santoso A, Lesage P, Dwiyono S, Sumarti S, Subandriyo S, Jousset P, Metaxian JP (2013) Analysis of the seismic activity associated with the 2010 eruption of Merapi Volcano, Java. *J Volcanol Geotherm Res* 261:153–170. <https://doi.org/10.1016/j.jvolgeores.2013.03.024>
- Burgisser A, Alletti M, Scaillet B (2015) Simulating the behavior of volatiles belonging to the C-O-H-S system in silicate melts under magmatic conditions with the software D-Compress. *Comput Geosci* 79:1–14
- Burgisser A, Bechon T, Chevalier L, Collombet M, Arbaret L, Forien M (2019) Conduit processes during the February 11, 2010 Vulcanian eruption of Soufrière Hills, Montserrat. *J Volcanol Geotherm Res* 373:23–35. <https://doi.org/10.1016/j.jvolgeores.2019.01.020>
- Burgisser A, Chevalier L, Gardner JE, Castro JM (2017) The percolation threshold and permeability evolution of ascending magmas. *Earth Planet Sci Lett* 470:37–47. <https://doi.org/10.1016/j.epsl.2017.04.023>
- Burgisser A, Poussineau S, Arbaret L, Druitt TH, Giachetti T, Bourdier JL (2010) Pre-explosive conduit conditions of the 1997 Vulcanian explosions at Soufrière Hills Volcano, Montserrat: I. Pressure and vesicularity distributions. *J Volcanol Geotherm Res* 194:27–41. <https://doi.org/10.1016/j.jvolgeores.2010.04.008>
- Cardoso SSS, Woods AW (1999) On convection in a volatile-saturated magma. *Earth Planet Sci Lett* 168:301–310. [https://doi.org/10.1016/S0012-821X\(99\)00057-6](https://doi.org/10.1016/S0012-821X(99)00057-6)
- Caricchi L, Pommier A, Pistone M, Castro J, Burgisser A, Perugini D (2011) Strain-induced magma degassing: insights from simple-shear experiments on bubble bearing melts. *Bull Volcanol* 73:1245–1257. <https://doi.org/10.1007/s00445-011-0471-2>
- Cassidy M, Manga M, Cashman K, Bachmann O (2018) Controls on explosive-effusive volcanic eruption styles. *Nat Commun* 9:2839. <https://doi.org/10.1038/s41467-018-05293-3>
- Chevrel MO, Cimarelli C, deBiasi L, Hanson JB, Lavallée Y, Arzilli F, Dingwell DB (2015) Viscosity measurements of crystallizing andesite from Tungurahua volcano (Ecuador). *Geochim Geophys Geosyst* 16:870–889. <https://doi.org/10.1002/2014GC005661>
- Clarke AB, Stephens S, Teasdale R, Sparks RSJ, Diller K (2007) Petrologic constraints on the decompression history of magma prior to Vulcanian explosions at the Soufrière Hills volcano, Montserrat. *J Volcanol Geotherm Res* 161:261–274. <https://doi.org/10.1016/j.jvolgeores.2006.11.007>
- Cole PD, Smith PJ, Stinton AJ, Odbert HM, Bernstein ML, Komorowski JC, Stewart R (2014) Chapter 5 Vulcanian explosions at Soufrière Hills Volcano, Montserrat between 2008 and 2010. *Geol Soc Lond Mem* 39(1):93–111
- Cole PD, Stinton AJ, Odbert HM, Bonadonna C, Stewart RC (2015) An inclined Vulcanian explosion and associated products. *J Geol Soc* 172(3):287–293
- Collombet M (2009) Two-dimensional gas loss for silicic magma flows: toward more realistic numerical models. *Geophys J Int* 177:309–318. <https://doi.org/10.1111/j.1365-246X.2008.04086.x>
- Colombier M, Wadsworth FB, Scheu B, Vasseur J, Dobson KJ, Cáceres F, Allabar A, Marone F, Schlepütz CM, Dingwell DB (2020) In situ observation of the percolation threshold in multiphase magma analogues. *Bull Volcanol* 82:32. <https://doi.org/10.1007/s00445-020-1370-1>
- Costa F, Andreastuti S, Bouvet de Maisonneuve C, Pallister JS (2013) Petrological insights into the storage conditions, and magmatic processes that yielded the centennial 2010 Merapi explosive eruption. *J Volcanol Geotherm Res* 261:209–235. <https://doi.org/10.1016/j.jvolgeores.2012.12.025>
- Couch S, Sparks RSJ, Carroll MR (2003) The kinetics of degassing-induced crystallization at Soufrière Hills volcano, Montserrat. *J Petrol* 44:1477–1502
- deGraffenried RL, Larsen JF, Graham NA, Cashman KV (2019) The influence of phenocrysts on degassing in crystal-bearing magmas with rhyolitic groundmass melts. *Geophys Res Lett* 46:5127–5136. <https://doi.org/10.1029/2018GL081822>
- Degruyter W, Bachmann O, Burgisser A, Manga M (2012) The effects of outgassing on the transition between effusive and explosive silicic eruptions. *Earth Planet Sci Lett* 349–350:161–170. <https://doi.org/10.1016/j.epsl.2012.06.056>
- Degruyter W, Parmigiani A, Huber C, Bachmann O (2019) How do volatiles escape their shallow magmatic hearth? *Philos Trans R Soc Lond Ser A* 377:20180017. <https://doi.org/10.1098/rsta.2018.0017>
- Drignon MJ, Bechon T, Arbaret L, Burgisser A, Komorowski JC, Caroline M, Hayden M, Yaputra R (2016) Preexplosive conduit conditions during the 2010 eruption of Merapi volcano (Java, Indonesia). *Geophys Res Lett* 43:11,595–11,602. <https://doi.org/10.1002/2016GL071153>
- Edmonds M, Aiuppa A, Humphreys M, Moretti R, Giudice G, Martin RS, Herd RA, Christopher T (2010) Excess volatiles supplied by mingling of mafic magma at an andesite arc volcano. *Geochim Geophys Geosyst* 11:4. <https://doi.org/10.1029/2009GC002781>
- Erdmann S, Martel C, Pichavant M, Bourdier JL, Champallier R, Komorowski JC, Cholik N (2016) Constraints from phase equilibrium experiments on pre-eruptive storage conditions in mixed magma systems: a case study on crystal-rich basaltic andesites from Mount Merapi, Indonesia. *J Petrol* 57:535–560. <https://doi.org/10.1093/petrology/egw019>
- Eychenne J, Le Pennec J-L, Troncoso L, Gouhier M, Nedelec J-M (2012) Causes and consequences of bimodal grain-size distribution of tephra fall deposited during the August 2006 Tungurahua eruption (Ecuador). *Bull Volcanol* 74:187–205. <https://doi.org/10.1007/s00445-011-0517-5>
- Farquharson J, Heap MJ, Varley NR, Baud P, Reuschlé T (2015) Permeability and porosity relationships of edifice-forming andesites: A combined field and laboratory study. *J Volcanol Geotherm Res* 297:52–68. <https://doi.org/10.1016/j.jvolgeores.2015.03.016>
- Gardner JE (2007) Bubble coalescence in rhyolitic melts during decompression from high pressure. *J Volcanol Geotherm Res* 166:161–176. <https://doi.org/10.1016/j.jvolgeores.2007.07.006>
- Gardner JE, Hilton M, Carroll MR (2000) Bubble growth in highly viscous silicate melts during continuous decompression from high pressure. *Geochim Cosmochim Acta* 64:1473–1483. [https://doi.org/10.1016/S0016-7037\(99\)00436-6](https://doi.org/10.1016/S0016-7037(99)00436-6)
- Gaunt HE, Burgisser A, Mothes PA, Browning J, Meredith PG, Criollo E, Bernard B (2020) Triggering of the powerful 14 July 2013 Vulcanian explosion at Tungurahua Volcano, Ecuador. *J Volcanol Geotherm Res* 392:106762. <https://doi.org/10.1016/j.jvolgeores.2019.106762>
- Giachetti T, Druitt TH, Burgisser A, Arbaret L, Galven C (2010) Bubble nucleation, growth and coalescence during the 1997 Vulcanian explosions of Soufrière Hills Volcano, Montserrat. *J Volcanol Geotherm Res* 193:215–231. <https://doi.org/10.1016/j.jvolgeores.2010.04.001>
- Gonnermann HM, Giachetti T, Flidner C, Nguyen CT, Houghton BF, Crozier JA, Carey RJ (2017) Permeability During Magma Expansion and Compaction. *J Geophys Res Solid Earth* 122:9825–9848. <https://doi.org/10.1002/2017JB014783>
- Guo Y, Wassgren C, Hancock B, Ketterhagen W, Curtis J (2013) Granular shear flows of flat disks and elongated rods without and with friction. *Phys Fluids* 25:063304. <https://doi.org/10.1063/1.4812386>
- Hall ML, Steele AL, Bernard B, Mothes PA, Vallejo SX, Douillet GA, Ramón PA, Aguaiza SX, Ruiz MC (2015) Sequential plug

- formation, disintegration by Vulcanian explosions, and the generation of granular Pyroclastic Density Currents at Tungurahua volcano (2013–2014), Ecuador. *J Volcanol Geotherm Res* 306:90–103. <https://doi.org/10.1016/j.jvolgeores.2015.09.009>
- Heap MJ, Farquharson JI, Baud P, Lavallée Y, Reuschlé T (2015) Fracture and compaction of andesite in a volcanic edifice. *Bull Volcanol* 77:55. <https://doi.org/10.1007/s00445-015-0938-7>
- Heap MJ, Lavallée Y, Petrakova L, Baud P, Reuschlé T, Varley NR, Dingwell DB (2014) Microstructural controls on the physical and mechanical properties of edifice-forming andesites at Volcán de Colima, Mexico. *J Geophys Res Solid Earth* 119:2013JB010521. <https://doi.org/10.1002/2013JB010521>
- Hidalgo S, Battaglia J, Arellano S, Steele A, Bernard B, Bourquin J, Galle B, Arrais S, Vásquez F (2015) SO₂ degassing at Tungurahua volcano (Ecuador) between 2007 and 2013: Transition from continuous to episodic activity. *J Volcanol Geotherm Res* 298:1–14. <https://doi.org/10.1016/j.jvolgeores.2015.03.022>
- Higgins MD, Roberge J (2003) Crystal size distribution of plagioclase and amphibole from Soufrière Hills Volcano, Montserrat: Evidence for dynamic crystallization-textural coarsening cycles. *J Petrol* 44:1401–1411
- Holtzman R, Szulcowski ML, Juanes R (2012) Capillary Fracturing in Granular Media. *Phys Rev Lett* 108:264504. <https://doi.org/10.1103/PhysRevLett.108.264504>
- Jenkins S, Komorowski J-C, Baxter PJ, Spence R, Picquout A, Lavigne F, Surono J (2013) The Merapi 2010 eruption: An interdisciplinary impact assessment methodology for studying pyroclastic density current dynamics. *J Volcanol Geotherm Res* 261:316–329
- Komorowski J-C, Jenkins S, Baxter PJ, Picquout A, Lavigne F, Charbonnier S, Gertisser R, Preece K, Cholik N, Budi-Santoso A, Surono J (2013) Paroxysmal dome explosion during the Merapi 2010 eruption: Processes and facies relationships of associated high-energy pyroclastic density currents. *J Volcanol Geotherm Res* 261:260–294
- Klug C, Cashman KV (1996) Permeability development in vesiculating magmas: implications for fragmentation. *Bull Volcanol* 58:87–100. <https://doi.org/10.1007/s004450050128>
- Kushnir ARL, Martel C, Bourdier JL, Heap MJ, Reuschlé T, Erdmann S, Komorowski JC, Cholik N (2016) Probing permeability and microstructure: Unravelling the role of a low-permeability dome on the explosivity of Merapi (Indonesia). *J Volcanol Geotherm Res* 316:56–71. <https://doi.org/10.1016/j.jvolgeores.2016.02.012>
- Kushnir ARL, Martel C, Champallier R, Arbaret L (2017) In situ confirmation of permeability development in shearing bubble-bearing melts and implications for volcanic outgassing. *Earth Planet Sci Lett* 458:315–326. <https://doi.org/10.1016/j.epsl.2016.10.053>
- La Spina G, de' Michieli Vitturi M, Clarke AB (2017) Transient numerical model of magma ascent dynamics: application to the explosive eruptions at the Soufrière Hills Volcano. *J Volcanol Geotherm Res* 336:118–139. <https://doi.org/10.1016/j.jvolgeores.2017.02.013>
- Larsen JF, Gardner JE (2000) Experimental constraints on bubble interactions in rhyolite melts: implications for vesicle size distribution. *Earth Planet Sci Lett* 180:201–214. [https://doi.org/10.1016/S0012-821X\(00\)00166-7](https://doi.org/10.1016/S0012-821X(00)00166-7)
- Laumonier M, Arbaret L, Burgisser A, Champallier R (2011) Porosity redistribution enhanced by strain localization in crystal-rich magmas. *Geology* 39:715–718. <https://doi.org/10.1130/G31803.1>
- Lindoo A, Larsen JF, Cashman KV, Oppenheimer J (2017) Crystal controls on permeability development and degassing in basaltic andesite magma. *Geology* 45:831–834. <https://doi.org/10.1130/G39157.1>
- Lyakhovskiy V, Hurwitz S, Navon O (1996) Bubble growth in rhyolitic melts: experimental and numerical investigation. *Bull Volcanol* 58:19–32. <https://doi.org/10.1007/s004450050122>
- Mangan M, Sisson T (2000) Delayed, disequilibrium degassing in rhyolite magma: decompression experiments and implications for explosive volcanism. *Earth Planet Sci Lett* 183:441–455. [https://doi.org/10.1016/S0012-821X\(00\)00299-5](https://doi.org/10.1016/S0012-821X(00)00299-5)
- Martel C, Iacono-Marziano G (2015) Timescales of bubble coalescence, outgassing, and foam collapse in decompressed rhyolitic melts. *Earth Planet Sci Lett* 412:173–185. <https://doi.org/10.1016/j.epsl.2014.12.010>
- Melnik O, Sparks RSJ (2002) Dynamics of magma ascent and lava extrusion at Soufrière Hills Volcano, Montserrat. *Geol Soc Lond Mem* 21:153–171. <https://doi.org/10.1144/GSL.MEM.2002.021.01.07>
- Michaut C, Bercovici D, Sparks RSJ (2009) Ascent and compaction of gas rich magma and the effects of hysteretic permeability. *Earth Planet Sci Lett* 282:258–267. <https://doi.org/10.1016/j.epsl.2009.03.026>
- Mueller S, Scheu B, Spieler O, Dingwell DB (2008) Permeability control on magma fragmentation. *Geology* 36:399–402. <https://doi.org/10.1130/G24605A.1>
- Murch AP, Cole PD (2019) Using microlites to gain insights into ascent conditions of differing styles of volcanism at Soufrière Hills Volcano. *J Volcanol Geotherm Res* 384:221–231. <https://doi.org/10.1016/j.jvolgeores.2019.07.022>
- Nadeau O, Williams-Jones AE, Stix J (2013) Magmatic-hydrothermal evolution and devolatilization beneath Merapi volcano, Indonesia. *J Volcanol Geotherm Res* 261:50–68. <https://doi.org/10.1016/j.jvolgeores.2013.04.006>
- Okumura S, Nakamura M, Nakano T, Uesugi K, Tsuchiyama A (2012) Experimental constraints on permeable gas transport in crystalline silicic magmas. *Contrib Mineral Petrol* 164:493–501. <https://doi.org/10.1007/s00410-012-0750-8>
- Oppenheimer C, Lomakina AS, Kyle PR, Kingsbury NG, Boichu M (2009) Pulsatory magma supply to a phonolite lava lake. *Earth Planet Sci Lett* 284:392–398. <https://doi.org/10.1016/j.epsl.2009.04.043>
- Oppenheimer J, Capponi A, Cashman KV, Lane SJ, Rust AC, James MR (2020) Analogue experiments on the rise of large bubbles through a solids-rich suspension: A “weak plug” model for Strombolian eruptions. *Earth Planet Sci Lett* 531:115931. <https://doi.org/10.1016/j.epsl.2019.115931>
- Oppenheimer J, Rust AC, Cashman KV, Sandnes B (2015) Gas migration regimes and outgassing in particle-rich suspensions. *Front Phys* 3. <https://doi.org/10.3389/fphy.2015.00060>
- Parmigiani A, Faroughi S, Huber C, Bachmann O, Su Y (2016) Bubble accumulation and its role in the evolution of magma reservoirs in the upper crust. *Nature* 532:492–495. <https://doi.org/10.1038/nature17401>
- Parmigiani A, Degruyter W, Leclaire S, Huber C, Bachmann O (2017) The mechanics of shallow magma reservoir outgassing. *Geochem Geophys Geosyst* 18:2887–2905. <https://doi.org/10.1002/2017GC006912>
- Preece K, Gertisser R, Barclay J, Berlo K, Herd RA, Edinburgh Ion Microprobe Facility (2014) Pre- and syn-eruptive degassing and crystallisation processes of the 2010 and 2006 eruptions of Merapi volcano, Indonesia. *Contrib Mineral Petrol* 168:1061. <https://doi.org/10.1007/s00410-014-1061-z>
- Preuss O, Marxer H, Ulmer S, Johannes W, Nowak M (2016) Special collection: rates and depths of magma ascent on Earth: degassing of hydrous trachytic Campi Flegrei and Phonolitic Vesuvius melts: experimental limitations and chances to study homogeneous bubble nucleation. *Am Mineral* 101:859–875. <https://doi.org/10.2138/am-2016-5480>
- Rust AC, Cashman KV (2004) Permeability of vesicular silicic magma: inertial and hysteresis effects. *Earth Planet Sci Lett* 228:93–107. <https://doi.org/10.1016/j.epsl.2004.09.025>
- Saar MO, Manga M, Cashman KV, Fremouw S (2001) Numerical models of the onset of yield strength in crystal-melt suspensions. *Earth Planet Sci Lett* 187:367–379. [https://doi.org/10.1016/S0012-821X\(01\)00289-8](https://doi.org/10.1016/S0012-821X(01)00289-8)

- Samaniego P, Le Pennec J-L, Robin C, Hidalgo S (2011) Petrological analysis of the pre-eruptive magmatic process prior to the 2006 explosive eruptions at Tungurahua volcano (Ecuador). *J Volcanol Geotherm Res* 199:69–84. <https://doi.org/10.1016/j.jvolgeores.2010.10.010>
- Shea T, Gurioli L, Larsen JF, Houghton BF, Hammer JE, Cashman KV (2010) Linking experimental and natural vesicle textures in Vesuvius 79 AD white pumice. *J Volcanol Geotherm Res* 192:69–84. <https://doi.org/10.1016/j.jvolgeores.2010.02.013>
- Shields JK, Mader HM, Pistone M, Caricchi L, Floess D, Pulitz B (2014) Strain-induced outgassing of three-phase magmas during simple shear. *J Geophys Res Solid Earth* 119:6936–6957. <https://doi.org/10.1002/2014JB011111>
- Stinton AJ, Cole PD, Stewart RC, Odbert HM, Smith P (2014) Chapter 7 The 11 February 2010 partial dome collapse at Soufrière Hills Volcano, Montserrat. *Geol Soc Lond Mem* 39(1):133–152
- Surono PJ, Pallister J, Boichu MM, Buongiorno F, Budisantoso A, Costa F, Andreastuti S, Prata F, Schneider D, Clarisse L, Humaida H, Sumarti S, Bignami C, Griswold J, Carn S, Oppenheimer C, Lavigne F (2012) The 2010 explosive eruption of Java's Merapi volcano—A '100-year' event. *J Volcanol Geotherm Res* 241–242: 121–135
- Takeuchi S, Tomiya A, Shinohara H (2009) Degassing conditions for permeable silicic magmas: implications from decompression experiments with constant rates. *Earth Planet Sci Lett* 283:101–110. <https://doi.org/10.1016/j.epsl.2009.04.001>
- Thomas ME, Neuberg JW, Collinson ASD (2019) Crystals, bubbles and melt: critical conduit processes revealed by numerical models. In: Gottsmann J, Neuberg J, Scheu B (eds) *Volcanic unrest : from science to society, advances in volcanology*. Springer International Publishing, Cham, pp 155–169. https://doi.org/10.1007/11157_2018_36
- van der Zwan FM, Chadwick JP, Troll VR (2013) Textural history of recent basaltic-andesites and plutonic inclusions from Merapi volcano. *Contrib Mineral Petrol* 166:43–63. <https://doi.org/10.1007/s00410-013-0864-7>
- Varas G, Ramos G, Géminard JC, Vidal V (2015) Flow and fracture in water-saturated, unconstrained granular beds. *Front Phys* 3:44. <https://doi.org/10.3389/fphy.2015.00044>
- Wadge G, Voight B, Sparks RSJ, Cole PD, Loughlin SC, Robertson REA (2014) Chapter 1 An overview of the eruption of Soufrière Hills Volcano, Montserrat from 2000 to 2010. *Geol Soc Lond Mem* 39(1):1.1–40
- Widiyantoro S, Ramdhan M, Métaxian JP, Cummins PR, Martel C, Erdmann S, Nugraha AD, Budi-Santoso A, Laurin A, Fahmi AA (2018) Seismic imaging and petrology explain highly explosive eruptions of Merapi Volcano, Indonesia. *Sci Rep* 8:13656. <https://doi.org/10.1038/s41598-018-31293-w>